UNIZIK JOURNAL OF ENGINEERING AND APPLIED SCIENCES (UJEAS)

Research Article

Response evaluation of iron ore sinter production rate based on ignition temperature and sintering time

C. I. Nwoye, C. N. Nwambu, C. C. Emekwisia, C. M. Ekwedigwe

Special Issue
A Themed Issue in Honour of Professor Clement Uche Atuanya on His retirement.

This themed issue pays tribute to Professor Clement Uche Atuanya in recognition of his illustrious career in Metallurgical and Materials Engineering as he retires from Nnamdi Azikiwe University, Awka. We celebrate his enduring legacy of dedication to advancing knowledge and his impact on academia and beyond through this collection of writings.

Edited by
Chinonso Hubert Achebe PhD.
Christian Emeka Okafor PhD.

UJEAS

UNIZIK JOURNAL OF ENGINEERING AND APPLIED SCIENCES

UNIZIK Journal of Engineering and Applied Sciences 3(3), September (2024), 958-973
Journal homepage: https://journals.unizik.edu.ng/index.php/ujeas
PRINT ISSN: 2992-4383 || ONLINE ISSN: 2992-4391

Response evaluation of iron ore sinter production rate based on ignition temperature and sintering time

C. I. Nwoye, C. N. Nwambu*, C. C. Emekwisia, and C. M. Ekwedigwe
Chemical Systems and Data Research Laboratory,
Department of Metallurgical and Materials Engineering, Nnamdi Azikiwe University, Awka, Nigeria
*Corresponding Author's E-mail: cn.nwambu@unizik.edu.ng

Abstract
The response of iron ore sinter production rate ϑ to the ignition temperature θ and sintering time τ has been evaluated. Iron ore was processed and sintered in a sinter reactor at basicity and ignition temperature range; 1.2 -5.0 and 864 - 1053^{0}C respectively. Ore particle size was < 1mm. The evaluative analysis was carried out using a derived model; $\vartheta = ß[(\underline{h}\tau^2 + \tau)\theta^{-N}]$, whose validity was based on the core model structure; $(\underline{h}\tau^2 + \tau) / n\vartheta \approx (\sqrt{\theta})$, in that both sides of the structure are correspondingly almost equal. ß, $\underline{h}$ and N are equalizing constants. Results generated from the derived and regression model prediction show significant similarities in the corresponding point and dimensional values with respect to experimental results. The standard error incurred in predicting the sinter production rate for every change in the influencing variables (relative to experimental results) is < 0.93%. This translates into a model confidence level above 99%. The sinter production rate per unit ignition temperature were 0.0081 and 0.0083 $tm^{-2}\ h^{-1}(^0C)^{-1}$, using experimental and model-predicted results respectively. The overall maximum deviation of the model-predicted production rate from experimental results was 8.12%. The derived model will predict the sinter production rate, within the experimental results range, on substituting into the model, values of the ignition temperature and residence time, providing the boundary conditions are considered.

Keywords: Iron ore, sinter production, ignition temperature, sintering time

1. Introduction

The sintering process is used to agglomerate a mix of iron ores (natural or synthetic), return fines, fluxes and coke, with a particle size of < 8 mm, so that the resulting sinter, with a screened size of 12-35 mm, can withstand pressure and temperature conditions in the blast furnace (Dawson, 1993; Goldring et al. 1989; Cores et al. 2010; Restrepo et al. 2008). Lu, (2015) reported that producing sinters of suitable quality at the lowest fuel rate and the highest productivity is the ultimate goal of most operations. Based on the foregoing, various fundamental researches and new technologies have been investigated by numerical and experimental methods in the last decade.

Investigation (Machida et al. 2009) has been carried on the segregation of solid fuels and charging condition with the aim at improving the heat distribution in sintering bed. Proposal was made (Zhou et al. 2015) for a novel technique involving three-layered bed structure, to study the effect of coke level, properties and combustion behaviour on NOx emission. Discussions (Kang et al. 2011) have been held in order to maximize the combustion efficiency and optimize the heat distribution, the effect of additional oxygen supply with an adjustment of injection position. The gaseous fuel injection technology was developed (Oyama et al. 2011), which provided a secondary combustion area above the original combustion area to produce high quality sinter without increasing the fuel

consumption. An intensive study numerically investigated (De Castro et al. 2014) gaseous fuel injection technology. On this basis, Iwami et al. (2013) employed the oxygen enrichment method with the aim to control the position of secondary combustion area. Addition of fuel externally to the raw ores was adopted and found to be beneficial to fuel combustion in both lab-scale sintering pot (Hou et al. 2011) and commercial sintering plant (Oyama et al. 2005). A laboratory sintering technique was developed (Loo and Wong, 2005). On the basis of the new technique, the effects of bed height, limestone, the level of return fines, mix moisture and suction on sintering behaviour were examined (Loo and Wong, 2005). Consequently, studied (Hou et al. 2015) were carried out on the influence of flame front on sintering production and quality.

Research (Abreu et al. 2015) has shown the possibility of adopting charcoal as supplementary fuel in the iron ore sintering process. The results amply show that the blend with 50% charcoal in the fuel mix was possible from both environmental and operational perspectives. However, the inaccuracy and hysteresis of manual adjustment of fuel segregation, fuel particles size, fuel distribution and even external operation are not able to satisfy the future automatic management of sinter production. Actually, on-line control has shown to be perfect and an alternative method to solve this problem. It is pertinent to note that, reliable and quick sintering performance indicators are required, considering that we need feedbacks to adjust operating parameters accordingly in time. The real-time visualization of sintering process "black-box" is a powerful support to the on-line controller. Therefore, connecting the process parameters and real sinter quality indices gives an urgent need for the on-line control process.

1.1 Raw mix

The raw mix that forms the sinter bed is comprised mainly of iron ores, coke, fluxes and return fines. The behaviour of the raw mix during sintering and the quality of the manufactured sinter depends largely on the chemical, granulometric and mineralogical composition of the iron ores. Understanding the impact of ore characteristics on sintering behaviour is important when it comes to selecting the most suitable raw mix for a given set of operating conditions. Research into the influence of the raw mix composition on sinter phases has determined the influence of basicity (CaO/SiO_2), temperature, thermal regime and Al_2O_3 and MgO contents on the ferrites content, total hematite, reoxidized hematite oxidized from magnetite, reducibility index (RI), reduction degradation index (RDI) and tumbler index (TI), porosity and coke rate (Yamaoka et al. 1974; Napoleao et al. 2003).

Figure 1 shows the assimilation of iron ore during sintering. The assimilation rate of iron ore increases with the ore porosity, which in turn increases with the combined water content. If the solid phase ratio in the melt formed at 1250 °C is established at 10%, in order to maintain the fluidity of the system, the nucleus must be formed by dense particles with a maximum diameter of 15 mm (Cores et al. 2013).

When sinters were manufactured with the individual ores, sintering properties (productivity, moisture, coke rate, RI, RDI, and TI) varied greatly with the iron ore type. When two ores were mixed, most of the sintering properties, except the RDI, were approximately equal to the weighted means of the individual ores. When mixes were made with increasing amounts of pisolite ore (Iwamoto et al. 1987), sinter productivity decreases on average by approximately 1.3% for each 10% mass pisolite ore increase, depending on the ore type replaced by the pisolite ore, and ensuring a higher coke rate and more moisture in the raw mix.

Later tests have shown that a coarser fuel is more economical, reinforces sinter production, improves RDI and lowers SO_2 emissions. The effect of the coke particle size (in the sinter bed) on productivity, coke consumption and sinter quality has been investigated (Hida et al. 1990). It was observed that coarser coke breeze fraction leads to a higher flame front speed and better combustion efficiency, while fine coke achieves poorer combustion efficiency, producing less heat and lowering the sintering temperature.

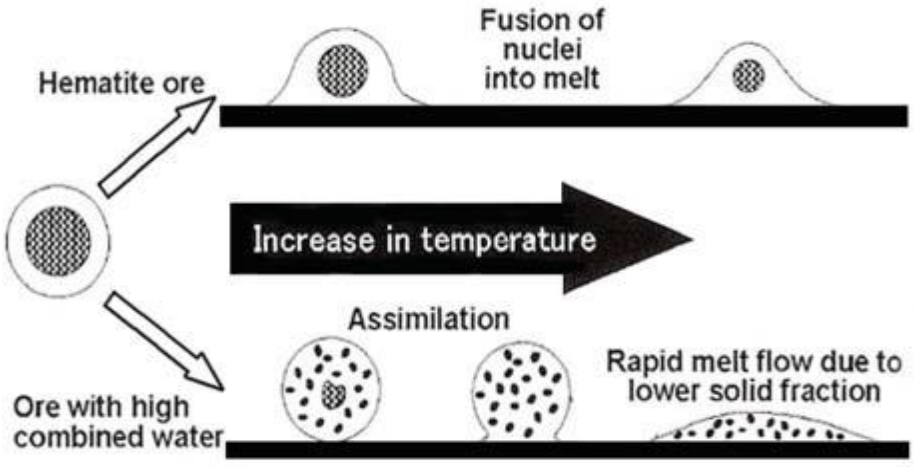

Figure 1: Assimilation of iron ore during sintering (Chen et al. 2022)

1.2 Granulation

Iron ore crushed to 5mm (as shown in Figure 2) appears dull, smooth and dense on one part, but shiny, fractured with fine and large pores on other parts. The complete granulation process, including the addition of moisture, granulation and insertion in the sintering machine takes approximately 30 minutes to 1 hour. Granulation is essential for the sintering of iron ores**.** This is because good sinter bed permeability largely determines the rate at which the process progresses and hence the productivity of the sinter plant. The first studies on the structure of granulated raw mixes were carried out at Nippon Steel Corporation (NSC) and coined the term "quasi-particle" [Lv et al.2010; Lv et al. 2010).

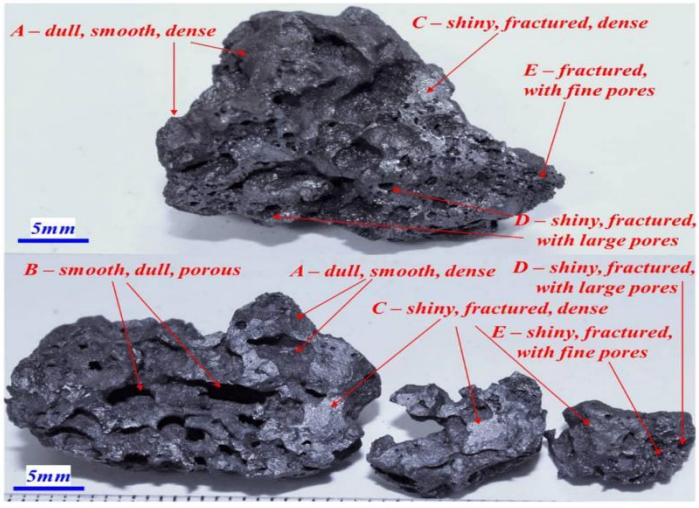

Figure 2: Iron ore sinter (Cheng et al. 2022)

A quasiparticle is composed of an iron ore nucleus, during which sinters remains partially unmelted, surrounded by finer ore grains with silica gangue and in the presence of high basicity (CaO/SiO_2). Figure 3 shows articles of > 0.7 mm act as nuclei while particles of < 0.2 mm act as adherent fines. The number of particles within the range 0.2 - 0.7 mm should be minimal because they affect the mix permeability in two different ways: (a) as nuclei they give rise to a smaller quasiparticle size, thereby lowering the bed permeability and (b) as adherent fines they are poorly bonded and easily separated from the dry particles (Litster and Water, 1988; Litster et al.1986). Raising the water

content of the raw mix during granulation enables intermediate particles to adhere to the coarse nuclei, but become quickly detached again during drying.

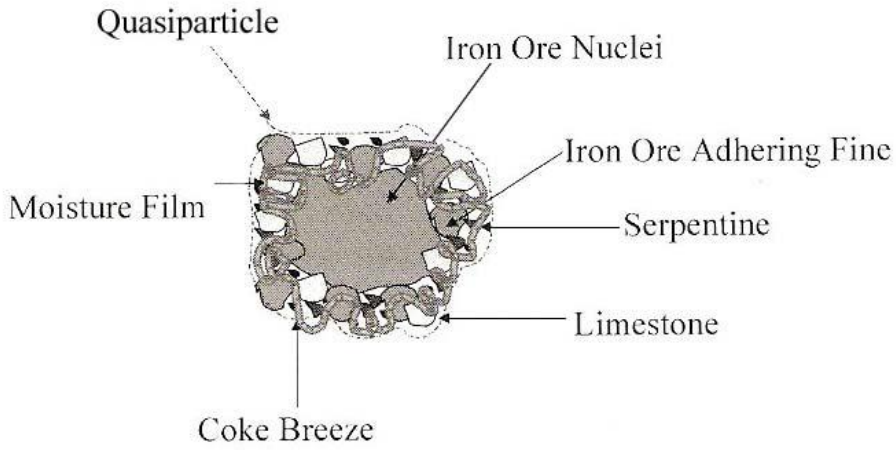

Figure 3**:** Quasi-particle schematic (Chen et al. 2022)

Research (Kawachi and Kasama, 2009) was carried out using 7 different iron ores to investigate the effect of microparticles on the optimum granulation moisture. An anionic polymer dispersant (APD) was found to accelerate micro-particles (<10μm and submicron size) dispersion in water with an increase in micro-particles content, resulting in strengthening the points of contact between the nuclear particles and fine particles or among the fine ones. The content of microparticles in each granulometric fraction for ores varied. The extent of the increase in microparticles by APD also varied with iron ore type, even though and the total amount of micro-particles was in the range 2 - 10% in all ores.

Investigations (Chemg et al. 2022) has shown (as in Figure 4) that in the process of change from the wet state to the dry state, microparticles concentrate at the water bridge and ultimately form a solid bridge, thereby producing the force which keeps the fine particles stuck to the nuclear particles. When APD is added, microparticles in the iron ore are dispersed into water, causing the increase in the amount of liquid phase. As a result, saturation degree increases, enabling ore optimal granulation with a lesser amount of water.

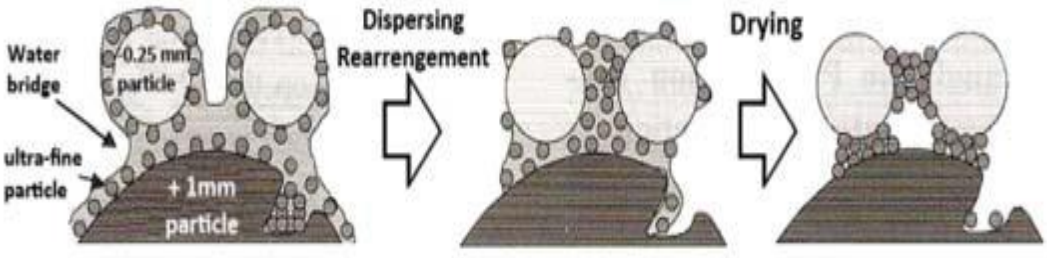

Figure 4: Behaviour of micro-particle on granulation (Cheng et al. 2022)

During sintering, ferrites form in the layer adheres to the nucleus due to the solid-liquid reaction between hematite and a $CaO\text{-}Fe_2O_3$ melt containing small amounts of SiO_2 and Al_2O_3. Adhesion is highly influenced by the moisture available for granulation (Litster and Water, 1988). Other factors such as the nature of the nucleus, particle shape and surface properties are of secondary importance.

1.3 Moisture content

The moisture content in the raw mix to be sintered is a very important parameter in the granulation stage of sintering. The process of adhering f ne particles to nuclei to form quasiparticles is very strongly influenced by the moisture available for granulation (total moisture minus moisture absorbed by sinter feed components) (Litster and Water, 1988). Maximum production is achieved with the optimum moisture addition, which is less than that required for maximum air permeability (Rankin, 1986) . It is customary to operate at about 0.85 times the requirement for condensation in the bottom layer of the bed after evaporating from the upper part as the flame front approached. Condensation is reported to take place during the first 2 min of sintering before the raw mix reaches its dew point temperature (Wild and Dixon, 1962).

Sintering time and productivity is largely influenced by flame front temperature because of its influence on flame front permeability. Results (Nakano et al. 2010) have shown that reducing flame front temperature is very beneficial to productivity because the resistance of the flame front to airflow is a function of gas velocity to the power of three. Air flow resistance is greatly increased by raising flame front temperature. This leads to increased sintering time and reduce productivity.

1.5 Relation between maximum flame front temperature and sinter structure

Investigation (Cheng et al. 2022) shows that when sintering is carried out at a temperature below 1300^0C, at around 1200^0C, a melt (consistently mainly of Fe_2O_3 and CaO) is generated in the sintering bed, and the iron oxide and fine particles are assimilated in the melt. If the melt penetrates the hematite grain, interfacial breakdown occurs, leaving a primary hematite (unmelted). This is considered beneficial for sintering because it improves the RI. Figure 5 indicates that when CaO and Al_2O_3 are assimilated in the melt, they react with the iron oxide and generates acicular calcium ferrite (of a size of less than 10 μm) containing Al_2O_3 and SiO_2 as solid dissolutions, according to the general reaction:

$$Fe_2O_3 + CaO + SiO_2 + Al_2O_3 \rightarrow SiO_2{\cdot}CaO{\cdot}(Fe.Al)_2O \quad (1)$$

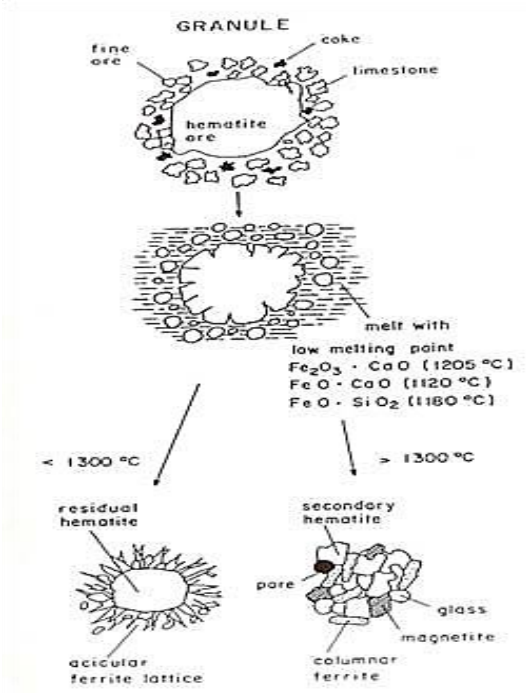

Figure 5: Development of sinter structure (Cheng et al. 2022)

1.6 Reactions in the sintering process

Metallurgists have reported (Loo et al. 2011) that during the sintering process, the temperature of raw mix is raised to achieve its partial melting and to produce a molten material which on cooling, crystallizes or solidifies into several mineral phases that agglomerate the structure as a whole. The energy for this process is supplied by combustion of the coke.

1.7 Effects of operating parameters on sinter strength

The effect of operating parameters on sinter strength has been investigated (Cheng et al. 2015). These parameters are fixed carbon content, sintering pressure, fuel category on sinter strength, combustion, and heat utilization efficiencies. Apart from accelerating the descending flame front, the increased sintering pressure also enhances the cooling rate of hot sinters which adversely affects the energy accumulation in the melting zone (Cheng et al, 2015). More so, higher sintering speed due to the increased air flow rate results from higher sintering pressure.

The amount of heat converted from chemical energy at certain fixed carbon content during the sintering process is determined by combustion efficiency (Cheng et al, 2015). Basically, accurately monitoring the local combustion efficiency in sintering bed is almost impossible. But for engineering applications, the waste gas composition at the outlet of sintering bed provides an available window for acknowledging combustion efficiency. Furthermore, the amount of effective energy applied to melting process, is largely determined by the heat utilization efficiency which is significantly affects the sintering process.

There exist two types of travelling fronts regarding filtration combustion. These are heat transfer front and reaction front (Yang et al. 2006). They propagate independently with their own speeds. Two typical travelling regimes are reaction leading and heat transfer leading, respectively. According to the filtration combustion theory, when the speeds of heat transfer front and reaction front are the same, heat accumulation effect in high temperature zone reaches to the maximum.

1.8 Previous models involving iron ore sintering and essential production parameters

Verification of numerical model and examination of the effects of coke content, air supply and fuel type on peak temperature, melting zone thickness and flame front speed have been carried out (Yang et al. 2006). Previous models (Zhou et al. 2012) have also been improved by considering detailed reactions, melting and solidification sub-models. The sensitivity analyses reveal that the bed bulk density, solid and gas thermal capacities, coke level and size and post-ignition air flow rate had significant influences on flame front speed and heat pattern. Further research (Zhao et al. 2012) by the scientists shows an improvement on computational model by integrating the granulation impact and two endothermic reactions into the heat treatment model. There has been a numerical investigated (Zhou et al. 2015) into the feasibility of utilizing spent ion exchange resin (SIER) in iron ore sintering process. The researchers established a 3-D model to examine the thermal conditions at different mass fractions of spent ion exchange resin (SIER). The mathematical modelling and optimization of two-layered sintering process for sinter quality and fuel efficiency using genetic algorithm has been carried out (Nath et al. 2016). On the other hand, Pahlevaninezhad (Mitterlehner et al. 2004) numerically investigated the sintering process by comprehensively considering the chemical reactions in gas and solid phase. In the course of the work, a wide range of parameters, including coke and limestone size, inlet air velocity and coke content were carefully examined.

A simulation model of the sintering process with special focus on the propagation velocity of the heat front through the bed has been developed (Mitterlehner et al. 2004). The effects of program-internal and user provided parameters were evaluated using this model. A modelling approach (Ahn et al. 2013) was proposed for a sintering bed using flow sheet process simulator as the starting point for studying the effect of flue gas recirculation on the sintering process. In the companion paper (Ahn et al. 2013), the details of the modelling cases and the corresponding results were reported.

The sinter production rate can be expressed in terms of tonnes per square meter of grate per hour and is calculated on the basis of production of + 5mm fraction following a shatter test (Nwokocha et al.2011). The sintering period is the time between the start of ignition and when the waste gas temperature attains a maximum. Based on the foregoing,

$$S_P \text{ rate} = \frac{60Ps}{\tau G_A} \quad (2)$$

Where

S_P rate = Sinter production rate ($tm^{-2} h^{-1}$)
P_S = Produced sinter (tonnes)
τ = Sintering time (mins.)
$\tau/60$ = Sintering time (hrs)
G_A = Grate area (m^2)

Research (Nwokocha et al.2011) has shown that the iron ore sinter production rate could be calculated based on the grate area, sintering time and quantity of produced sinter. Interestingly, the grate area is dependent on some other parameters such as the dimensions/ configuration of the sintering equipment. However, no existing mathematical expression or model has predicted the iron ore sinter production rate, putting into consideration, the vital roles played by the ignition temperature, apart from the sintering duration and quantity of produced sinter. This has amply prompted the need for the present work to fill in the gap.

The present work aims at deriving an empirical model to ascertain the possibility of predicting the iron ore sinter production rate, based on the ignition temperature (in place of quantity of produced sinter and grate area) and sintering time. The model if derived, shall predict the sinter production rate within the experimental result range, providing the input parameters are within the boundary condition

2. Materials and methods

2.1 Preparation of the mix component

The iron ore concentrates, limestone and coke breeze were crushed, ground and dried and sieved to < 1mm particle size. All the materials were carefully mixed and granulated by adding water to achieve the same moisture content in the granulation drum for 5 min. For every test, 350 g hearth ore and approximate 10 kg raw mix after granulation were fed into the sintering reactor at a temperature range 1000 -1200^{0}C The mix was ignited using a mixture of natural gas and air in 60 seconds. At ignition, the pressure was kept constant at 6Kpa. After ignition, the pressure was increased to 1.2 Mpa. The air flow rate was approximately controlled by varying sintering pressure and keeping cold permeability unchanged. Measurements were carried out to evaluate productivity and porosity of the sinters. Series of other tests such as shatter test and reducibility test were also carried out including tumble tests to determine the physical strength of the sinter and chemical analysis to determine FeO, Fe_2O_3, CaO, SiO_2 & CaO free contents. The steps for testing mineralization were agglomeration, roasting and mineralogical analysis. The basicity (CaO/SiO_2) was varied from 1.2 – 5.0. All materials used were analyzed using Atomic Absorption Spectrometer (AAS). Results of the chemical analyses are shown in Table 1.

Table 1: Chemical Analysis of the materials used (wt. %)

Material used	FeO	Fe_2O_3	SiO_2	AL_2O_3	MgO	CaO	MnO	Fe_{tot}	S	
Itapke Iron Ore Concentrates	1.0	88.9	8.8	0.8	-	0.20	-	64.4	0.9	
Mixture of 50% Jakuru Limestone	-	0.35	4.45	0.30	10.7	42.0	-	0.175	-	
Sinter Returns	9.10	59.3	7.5	0.9	1.7	10.1	0.7	48.8	0.1	
	FeO	Fe_2O	MnO	SiO	AL_2O_3	C	M_2O	S_{org}	FeS	SO_3
Coke Breeze	-	3.2	0.21	6.0	3.2	1.4	0.6	0.25	0.23	0.21

A base case sinter was used to examine the influence of ignition temperature on the physical and metallurgical properties of the sinter. The materials used and quantity is given in Table 2

Table 2: Proportions of the raw materials in the base case sinter mixture

Material used	mass (kg)	mass (%)
Itakpe iron ore	38.37%	25.58
Return fines	37.5	25.00
Coke Breeze	6.60	4.04
Limestone	9.24	6.16
Dolomite	10.94	7.29
Silica	0.30	0.2
Water	7.65ml	5.10
$FeCl_3$	1.4ml	0.69

2.2 Sintering process

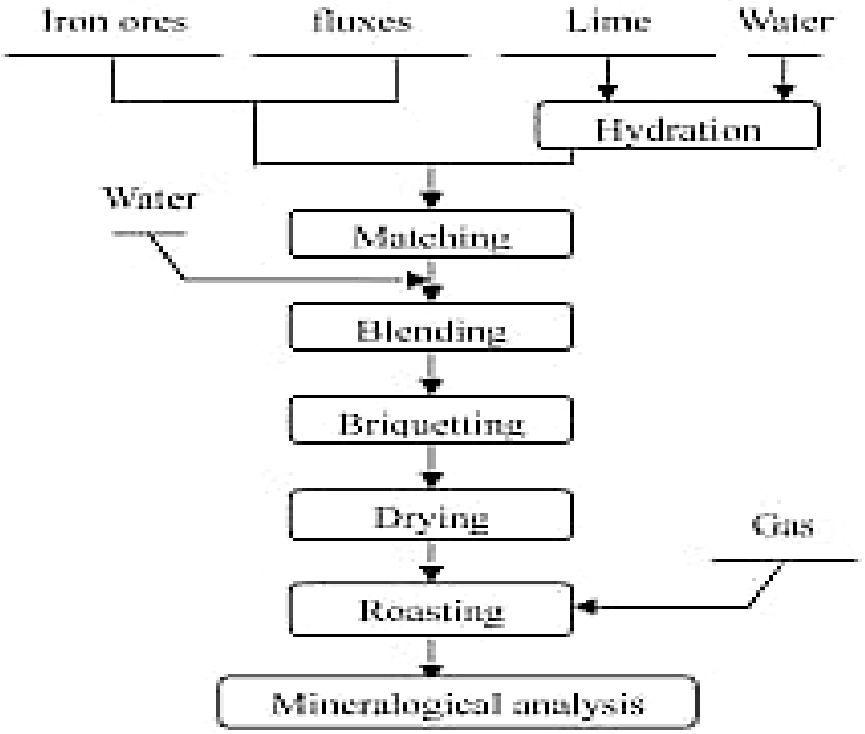

Figure 6: Experimental flow of mini-sintering process

Figure 6 shows the steps involving iron ore sinter production from raw material processing through matching to roasting, and terminating in mineralogical analysis. However, mineralogical analysis follows cooling to enable handling.

3. Model Derivation

Table 1: Variation of sinter production rate with sintering time and ignition temperature, while basicity is constant

(τ) (mins.)	ϑ ($tm^{-2}h^{-1}$)	θ (^0C)	(β)
27.03	25.01	864	5.0
26.58	25.50	880	5.0
26.10	26.03	897	5.0
27.26	25.23	905	5.0
28.75	24.62	938	5.0
28.41	25.39	965	5.0
28.13	26.01	987	5.0
28.31	25.82	1000	5.0
29.03	25.02	1053	5.0

Computational analysis of the experimental results shown in Table 1, resulted to Table 2 which indicate that;

$$\frac{(Ъ\tau^2 + \tau)}{n\vartheta} \approx (\sqrt{\theta})^{ɱ} \quad (3)$$

$$\vartheta = \frac{(Ъ\tau^2 + \tau)}{n(\sqrt{\theta})^{ɱ}} \quad (4)$$

$$\vartheta = ß[(Ъ\tau^2 + \tau)\theta^{-N}] \quad (5)$$

The empirical model in (4) or in a more simplified way (5) predicts the sinter production rate of iron oxide ore based on the sintering duration and ignition temperature of range 27.03 – 31.1 mins. and 864 -1100^{0}C respectively. The variables τ, ϑ, θ, and β are sintering duration (mins.) sinter production rate ($tm^{-2}h^{-1}$), ignition temperature (^0C) and basicity respectively. The derived model is referred to as Nwoye`s Model for evaluating the sinter production rate of iron ore based on ignition temperature and sintering time or Nwoye`s SIPRATE Model. The equalizing constants; ɱ, Ъ and n are 1.8x 10^{-4}, 2 x10^{-6} and 1.0795 respectively, while N and ß are 0.9x 10^{-4} (root figure (0.5) multiplied by ɱ) and 0.9264 (inverse of n) respectively. The software (Nwoye et al. 2008) was used in generating the equalizing constants. The interaction between the constants and associated variables ensured same units on both sides of the model.

It could be recalled that the sinter production rate evaluated from equation (4), using the conventional formular (Wild, 1962) are based on values of the sintering time and grate area recorded during the associated experiment.

Substituting (2) into (5), gives that;

$$\frac{60Ps}{\tau G_A} = ß[(Ъ\tau^2 + \tau)\theta^{-N}] \quad (6)$$

The expression in (6) shows that S_P rate = ϑ. This happens if the numerical differential between the expressions in (2) and (5) are negligible or zero. It is therefore instructive to state that any of the parameters in (6) can be evaluated, if other values are known.

4. Results and Discussion

4.1 Boundary and Initial Conditions

Consider iron ore particles, interacting with added limestone, CaO and fluxes and coke breeze. Sinter production rate resulted from the impact of ignition temperature, resident time and pressure on the mix. During the model derivation,

the considered range of ignition temperature, sintering time and sinter production rate are 864 -1053^{0}C, 26.1 – 29.03 mins. and 24.62 – 26.03 tm^{-2} h^{-1} respectively.

Table 2: Variation of both sides of the core model structure; $(Ъ\tau^2 + \tau)/n\vartheta$ with $(\sqrt{\theta})^{ɱ}$

$(Ъ\tau^2 + \tau)/n\vartheta$	$(\sqrt{\theta})^{ɱ}$	Differential
1.0012	1.000608	0.00059
0.9656	1.000610	-0.03501
0.9289	1.000612	-0.07171
1.0009	1.000613	0.00029
1.0818	1.000616	0.08118
1.0366	1.000619	0.03598
1.0019	1.000621	0.00128
1.0157	1.000622	0.01508
1.0749	1.000627	0.07427

4.2 Model Validity

The validity of the model in (5) is deeply rooted in the core model structure; $(Ъ\tau^2 + \tau)/n\vartheta \approx (\sqrt{\theta})^{ɱ}$ expressed in (3). This is so because both sides of the model structure are correspondingly almost equal as shown in Table 2, which gives numerical confirmation. This table was generated through evaluation of experimental results in Table 1. Table 2 also indicates very negligible differentials between the corresponding sides of the structure components, emphasizing the functionality of the derived model.

The derived model was also validated by comparing the predicted results with the experimental, through graphical, statistical and deviational analysis.

4.2.1 Graphical Analysis

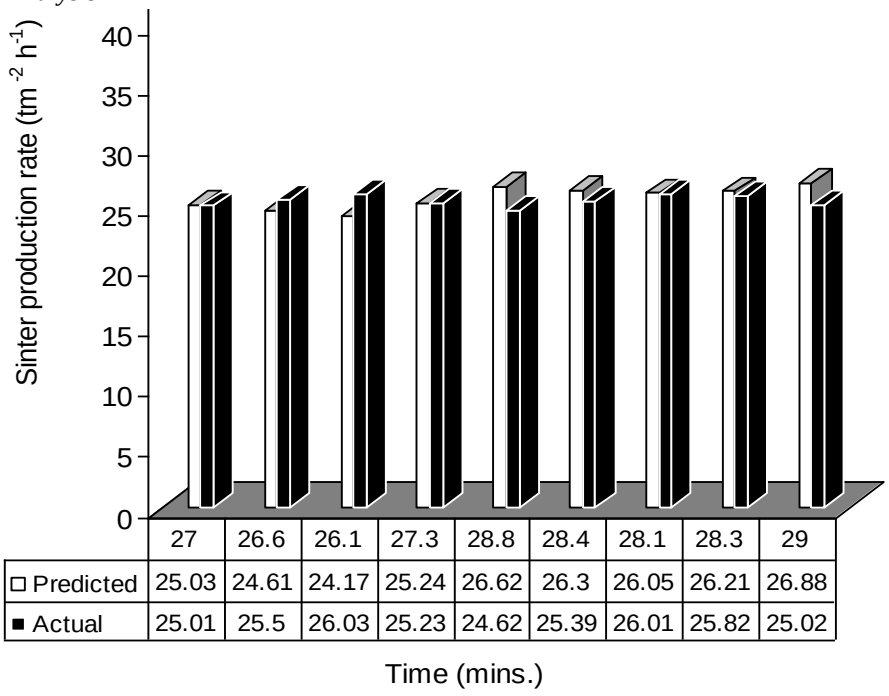

Figure 7: Comparison of sinter production rate (relative to sintering time) as evaluated from actual results and derived model

Analysis of Figures 7 and 8 reveals near equal heights of bars of sinter production rates, relative to sintering time and ignition temperature, representing the experimental and model-predicted results. These figures also show point-to-point values of the experimental and model-predicted results, for every elapsed resident time and ignition temperature applied. The bars are also characterized by proximate corresponding point values.

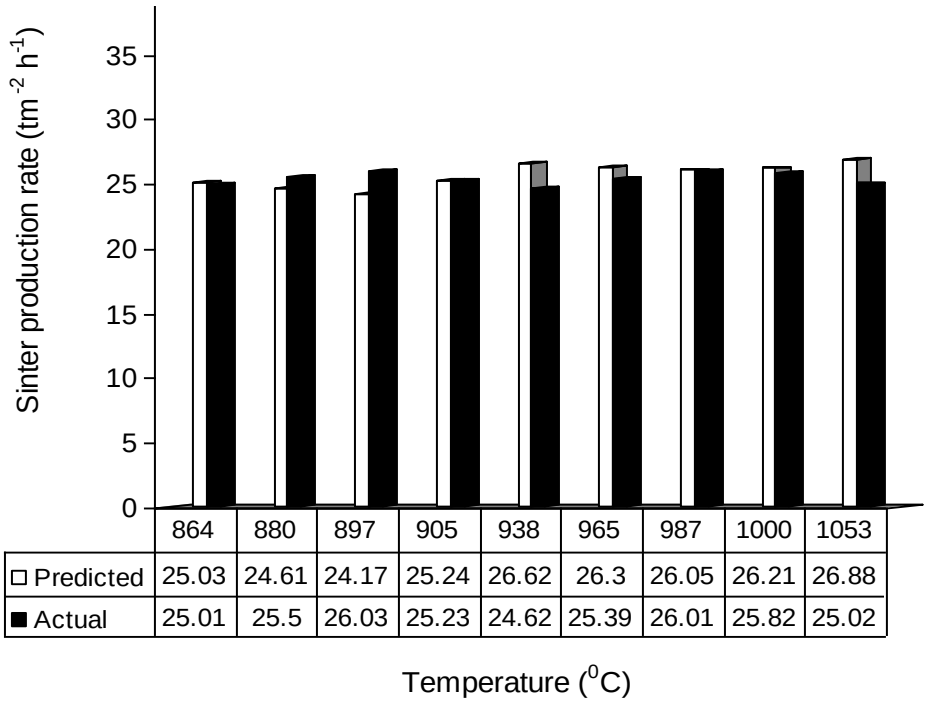

	864	880	897	905	938	965	987	1000	1053
□ Predicted	25.03	24.61	24.17	25.24	26.62	26.3	26.05	26.21	26.88
■ Actual	25.01	25.5	26.03	25.23	24.62	25.39	26.01	25.82	25.02

Figure 8: Comparison of sinter production rate (relative to ignition temperature) as evaluated from actual results and derived model

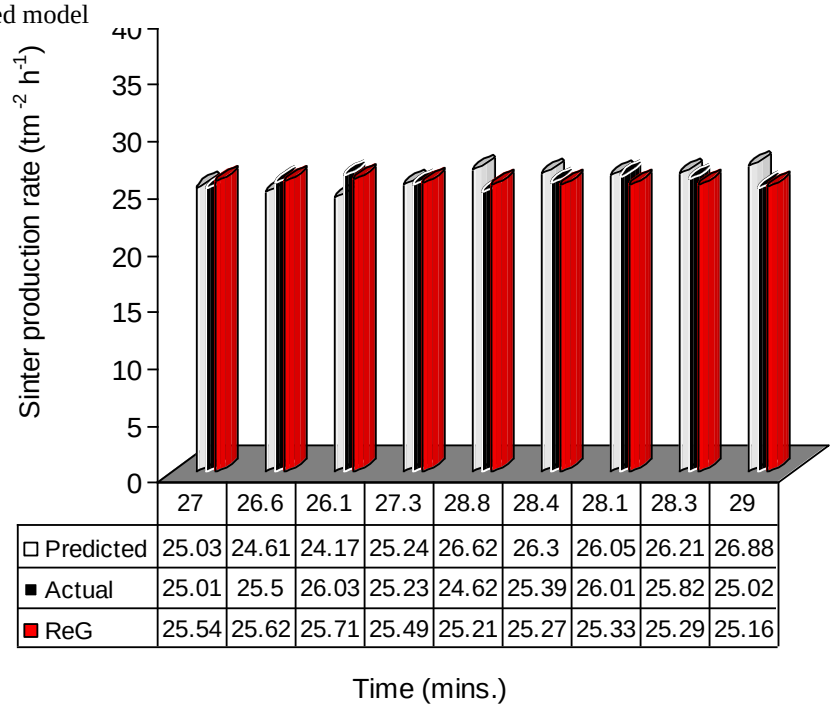

	27	26.6	26.1	27.3	28.8	28.4	28.1	28.3	29
□ Predicted	25.03	24.61	24.17	25.24	26.62	26.3	26.05	26.21	26.88
■ Actual	25.01	25.5	26.03	25.23	24.62	25.39	26.01	25.82	25.02
■ ReG	25.54	25.62	25.71	25.49	25.21	25.27	25.33	25.29	25.16

Figure 9: Comparison of sinter production rate (relative to sintering time) as evaluated from actual results, derived model and regression model

Figure 9 share similarities with Figure 7 in terms of the heights of bars and corresponding point values. Figure 10 indicates closely aligned curves from experimental, derived model and regression model-predicted results. The only significant difference between Figures 7 & 8 and Figures 9 & 10 is the presence of regression results, which pose as a standard model result predicted by the computer. Generated results show that the level of discrepancy between the plotted regression values and the other aligned results determines the functionality and acceptability of the derived model.

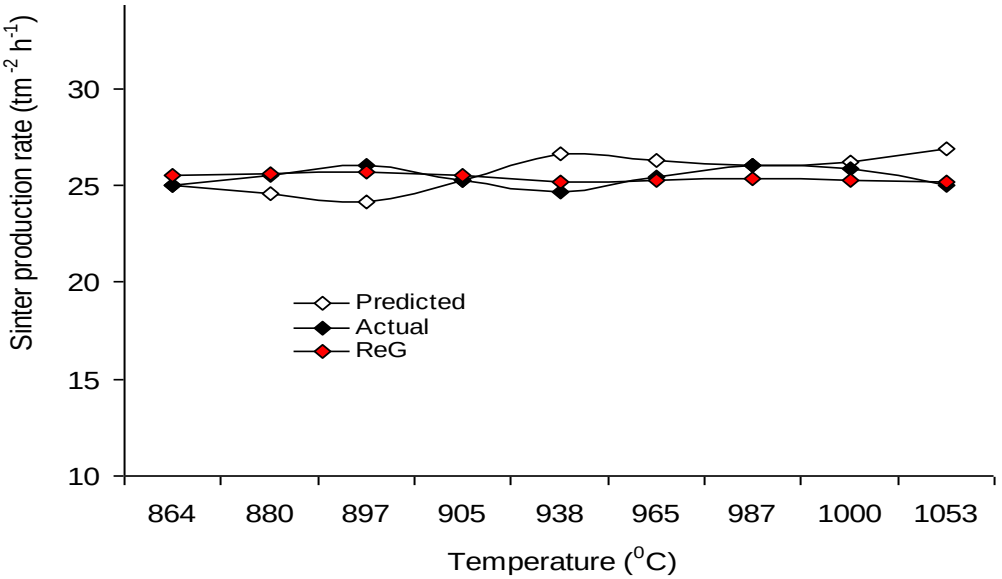

Figure 10: Comparison of sinter production rate (relative to ignition temperature) as evaluated from actual results, derived model and regression model

4.2.2 Statistical Analysis

Comparative analysis of results generated from the model and experiment shows that the standard errors incurred in generating the model-predicted results of sinter production rate (for every input of ignition temperature and sintering duration) relative to those from experiment is < 0.93%. This gives a model confidence level above 99%.

4.2.3 Deviation Analysis

Table 3: Differential between experimentally determined and model-predicted sinter production rate

(ϑ)	$\Delta\vartheta = \vartheta_M - \vartheta_E$
25.01	0.02
25.50	-1.86
26.03	0.01
25.23	2.00
24.62	0.91
25.39	0.04
26.01	0.39
25.82	1.86
25.02	-

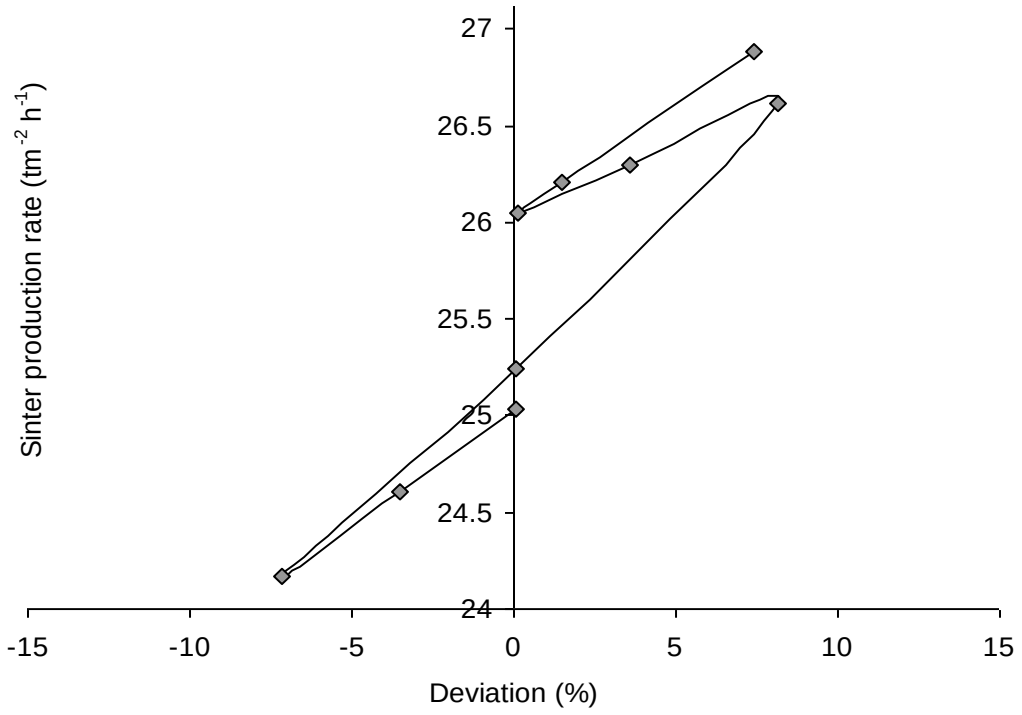

Figure 11: Variation of model-predicted sinter production rate with its corresponding deviation from experimental results

The differentials between experimentally determined and corresponding model-predicted sinter production rate is shown in Table 3. Comparative analysis of both sides of table shows negative and positive differentials, which indicate decreased and increased model-predicted values respectively, relative to corresponding experimental results.

Figure11 shows that the maximum deviation of the model-predicted sinter production rate from the corresponding experimental results is < 8.2%, translating into a model confidence level above 91%. Evaluated results plotted in the figure show that the least and highest magnitude of deviations of the model-predicted sinter production rate is 0.04 and 8.12% respectively. These deviations correspond to sinter production rate: 25.24 & 26.62 tm^{-2} h^{-1}, sintering time: 27.26 & 28.75mins. and ignition temperature: 905 & 938^{0}C respectively. Based on evaluated results, the overall model confidence level places at between 91 and 99%.

The deviation Dv, of model-predicted sinter production rate from the corresponding experimental result was evaluated from the expression.

$$D_v = \left[\frac{\vartheta_m - \vartheta_E}{\vartheta_E}\right] \times 100 \qquad (7)$$

Where

ϑ_E and ϑ_m are sinter production rates evaluated from experimental and model-predicted results respectively. Correction factor which overcomes the deviation is calculated as the negative of equation (7);

$$C_f = -\left[\frac{\vartheta_m - \vartheta_E}{\vartheta_E}\right] \times 100 \qquad (8)$$

The model-predicted results could be numerically placed at equality with experimental results by introducing a correction factor which is numerically equal, but of negative sign to the sign of the evaluated deviation of the model-predicted results.

Sinter production rate per unit ignition temperature ϑ_θ tm^{-2} $h^{-1}(^0C)^{-1}$ was calculated from the expression;

$$\vartheta_\theta = \vartheta / \theta \quad (9)$$

Re-written as

$$\vartheta_\theta = \Delta\vartheta / \Delta\theta \quad (10)$$

The expression (10), is detailed as

$$\vartheta_\theta = \vartheta_2 - \vartheta_1 / \theta_2 - \theta_1 \quad (11)$$

Where

$\Delta\vartheta_\theta$ = Change in the sinter production rate ϑ_2, ϑ_1 at two ignition temperatures θ_2, θ_1

On plotting points (864, 25.01) & (987, 26.01) and (864, 25.03) & (987, 26.05) shown in Figure 10, designated as (θ_1, ϑ_1) and (θ_2, ϑ_2) for experimental and derived model-predicted results, and substituting them into the expression (11), gives the slopes: 0.0081 and 0.0083 tm^{-2} $h^{-1}(^0C)^{-1}$, as their respective sinter production rate per unit ignition temperature.

Conclusion

The response of iron ore sinter production rate to the ignition temperature and sintering time was evaluated. The evaluative analysis was carried out using a derived model; $\vartheta = ß[(Ъ\tau^2 + \tau)\theta^{-N}]$, whose validity was based on the core model structure; $(Ъ\tau^2 + \tau) / n\vartheta \approx (\sqrt{\theta})$, in that both sides of the structure are correspondingly almost equal. Results generated from the derived and regression model prediction agree with experimental values. The standard error incurred in predicting the sinter production rate for every change in the influencing variables (relative to experimental results) is < 0.93%. This translates into a model confidence level above 99%. The sinter production rates per unit ignition temperature are 0.0081 and 0.0083 tm^{-2} $h^{-1}(^0C)^{-1}$, using experimental and model-predicted results respectively. The overall maximum deviation of the model-predicted production rate from experimental results was 8.12%. The derived model will predict the sinter production rate, within the experimental results range, on substituting into the model, values of the ignition temperature and residence time, providing the boundary conditions are considered.

References

Abreu, G.C., de Carvalho Jr, J.A., da Silva, B.E.C. and Pedrini, R.H., 2015. Operational and environmental assessment on the use of charcoal in iron ore sinter production. *Journal of Cleaner Production*, *101*, pp.387-394.

Ahn, H., Choi, S. and Cho, B., 2013. Process simulation of iron ore sintering bed with flue gas recirculation: part 1–modelling approach. *Ironmaking & Steelmaking*, *40*(2), pp.120-127.

Ahn, H., Choi, S. and Cho, B., 2013. Process simulation of iron ore sintering bed with flue gas recirculation: Part 2–Parametric variation of gas conditions. *Ironmaking & Steelmaking*, *40*(2), pp.128-137.

Cheng, S., Hayes, P.C. and Jak, E., 2022. Iron ore sinter macro-and micro-structures, and their relationships to breakage characteristics. *Minerals*, *12*(5), p.631.

Cheng, Z., Yang, J., Zhou, L., Liu, Y. and Wang, Q., 2016. Sinter strength evaluation using process parameters under different conditions in iron ore sintering process. *Applied Thermal Engineering*, *105*, pp.894-904.

Cores A, Verdeja, L. F. Ferreira, S. Ruiz-Bustinza I. and Mochon. J. 2013. Iron Ore Sintering. Part 1: Theory and Practice of Sintering Process. Dyna, year 80, Nro. 180:152-171.

Cores, A., Babich, A., Muñiz, M., Ferreira, S. and Mochon, J., 2010. The influence of different iron ores mixtures composition on the quality of sinter. *ISIj International*, *50*(8), pp.1089-1098.

Dawson, P. R., 1993 *Ironmaking Steelmaking*, vol. 20, pp.137-143.

De-Castro, J.A., 2014. Model predictions for new iron ore sintering process technology based on biomass and gaseous fuels. *Advanced Materials Research*, *918*, pp.136-144.

Formoso, A., Moro, A., Fernández Pello, G., Menéndez, J.L., Muñiz, M. and Cores, A., 2003. Influence of nature and particle size distribution on granulation of iron ore mixtures used in a sinter strand. *Ironmaking & steelmaking*, *30*(6), pp.447-460.

Gan, M., Fan, X. and Chen, X., 2015. Calcium ferrit generation during iron ore sintering—crystallization behavior and influencing factors. *Adv Topic Crystal Tech*, *301*, pp.301-320.

Goldring, D. C., Juckes L. M. and Fray, T. A. T., 1989. *Proc. 5th Int. Symp. on Agglomeration, Brighton*, United Kingdom, , The Institution of Chemical Engineers (ICHEME), pp. 425-439.

Hida, Y., Okazaki, J. and Nakamura, K., *Proc. 6th Int. Iron and Steel Cong*., Nagoya, Japan, ISIJ, pp. 40-47, 1990.

Hou, P., Choi, S., Choi, E. and Kang, H., 2011. Improved distribution of fuel particles in iron ore sintering process. *Ironmaking & Steelmaking*, *38*(5), pp.379-385.

Iwami, Y., Yamamoto, T., Higuchi, T., Nushiro, K., Sato, M. and Oyama, N., 2013. Effect of oxygen enrichment on sintering with combined usage of coke breeze and gaseous fuel. *ISIJ international*, *53*(9), pp.1633-1641.

Kang, H., Choi, S., Yang, W. and Cho, B., 2011. Influence of oxygen supply in an iron ore sintering process. *ISIJ international*, *51*(7), pp.1065-1071.

Kawachi, S. and Kasama, S., 2009. Quantitative effect of micro-particles in iron ore on the optimum granulation moisture. *ISIJ international*, *49*(5), pp.637-644.

Litster, J.D. and Waters, A.G., 1988. Influence of the material properties of iron ore sinter feed on granulation effectiveness. *Powder Technology*, *55*(2), pp.141-151.

Litster, J.D., Waters, A.G. and Nicol, S.K., 1986. A model for the size distribution of product from a granulating drum. *Transactions of the Iron and Steel Institute of Japan*, *26*(12), pp.1036-1044.

Loo, C.E. and Wong, D.J., 2005. Fundamental factors determining laboratory sintering results. *ISIJ international*, *45*(4), pp.449-458.

Loo, C.E., Matthews, L.T. and O'dea, D.P., 2011. Lump ore and sinter behaviour during softening and melting. *ISIJ international*, *51*(6), pp.930-938.

Lu. L. 2015. Important iron ore characteristics and their impacts on sinter quality – a review. Minerals & Metallurgical process, 32, 88-96.

Lv, X., Bai, C., Qiu, G., Zhang, S. and Hu, M., 2010. Moisture capacity: definition, measurement, and application in determining the optimal water content in granulating. *ISIJ international*, *50*(5), pp.695-701.

Lv, X.W., Bai, C.G., Zhou, C.Q., Xie, H. and Shi, R.M., 2010. New method to determine optimum water content for iron ore granulation. *Ironmaking & Steelmaking*, *37*(6), pp.407-413.

Machida, S. Higuchi, T. Oyama, N. Sato, H. Takeda, K. Yamashita, K. Tamura. K. 2009. Optimization of coke breeze segregation in sintering bed under high pisolite ore ratio. ISIJ International, 49, 667-675.

Mitterlehner, J., Löffler, G., Winter, F., Hofbauer, H., Schmid, H., Zwittag, E., TH, B., Pammer, O. and Stiasny, H., 2004. Modeling and simulation of heat front propagation in the iron ore sintering process. *ISIJ international*, *44*(1), pp.11-20.

Nakano, M., Katayama, K. and Kasama, S., 2010. Theoretical characterization of steady-state heat wave propagating in iron ore sintering bed. *ISIJ international*, *50*(7), pp.1054-1058.

Napoleão, A., Pinheiro, P., Caparoli, L. and Oliveira, D., 2003. LA, Fujikawa, L. and Vervenee, R. In *Proc. 3rd Int. Conf. on Sci. and Tech. of Ironmaking, VDEh, Düsseldorf, Germany* (pp. 127-132).

Nath, N.K. and Mitra, K., 2005. Mathematical modeling and optimization of two-layer sintering process for sinter quality and fuel efficiency using genetic algorithm. *Materials and manufacturing processes*, *20*(3), pp.335-349.

Nwoye C. I. (2008). Data Analytical Memory; C-NIKBRAN

Nwoye, C.I., Nnuka, E.E., Nwokocha, V.O. and Nwakpa, S.O., 2013. Particulate sintering of iron ore and empirical analysis of sintering time based on coke breeze input and ignition temperature. *IOSR Journal of Mechanical and Civil Engineering*, *7*(4), pp.42-51.

Oyama, N., Iwami, Y., Yamamoto, T., Machida, S., Higuchi, T., Sato, H., Sato, M., Takeda, K., Watanabe, Y., Shimizu, M. and Nishioka, K., 2011. Development of secondary-fuel injection technology for energy reduction in the iron ore sintering process. *ISIJ international*, *51*(6), pp.913-921.

Oyama, N., Sato, H., Takeda, K., Ariyama, T., Masumoto, S., Jinno, T. and FUJII, N., 2005. Development of coating granulation process at commercial sintering plant for improving productivity and reducibility. *ISIJ international*, *45*(6), pp.817-826.

Pahlevaninezhad, M., Emami, M.D. and Panjepour, M., 2014. The effects of kinetic parameters on combustion characteristics in a sintering bed. *Energy*, *73*, pp.160-176.

Rankin, W. J., *Proc. 2nd Int. Symp. on "Benefaction and Agglomeration"*, 1986, Bhubaneswar, India, Institute of Metals, pp. 107-117.

Restrepo-Baena, O.J., Vásquez Jiménez, C.F. and Bustamante Rúa, M.O., 2008. Influencia del pH en las propiedades pigmentarias de la goetita sintética. *Dyna*, *75*(155), pp.163-170.

Wild, R. and Dixon, K. G., *Proc. 1st Int. Symp. On Agglomeration*, 1962, New York, USA, Wiley-Interscience, pp. 565-580.

Yamaoka, Y., Nagaoka, S., Yamada, Y. and Ando, R., 1974. Effect of gibbsite on sintering property and sinter quality. *Transactions of the Iron and Steel Institute of Japan*, *14*(3), pp.185-194.

Yang, W., Choi, S., Choi, E.S., Ri, D.W. and Kim, S., 2006. Combustion characteristics in an iron ore sintering bed—evaluation of fuel substitution. *Combustion and Flame*, *145*(3), pp.447-463.

Zhao, J.P., Loo, C.E. and Dukino, R.D., 2015. Modelling fuel combustion in iron ore sintering. *Combustion and Flame*, *162*(4), pp.1019-1034.

Zhou, G.W. Zhong, W.Q. Zhao, H.C. Jin, B.S. Wang, T.C. Liu. F. 2015 Heat transfer of spent ion exchange resin in iron ore sintering process. Applied Thermal Engineering, 88, 258-264.

Zhou, H., Liu, Z., Cheng, M., Liu, R. and Cen, K., 2015. Effect of flame-front speed on the pisolite-ore sintering process. *Applied Thermal Engineering*, *75*, pp.307-314.

Zhou, H., Liu, Z., Cheng, M., Zhou, M. and Liu, R., 2015. Influence of coke combustion on NO x emission during iron ore sintering. *Energy & Fuels*, *29*(2), pp.974-984.

Zhou, H., Zhao, J.P., Loo, C.E., Ellis, B.G. and Cen, K.F., 2012. Numerical modeling of the iron ore sintering process. *ISIJ international*, *52*(9), pp.1550-1558.

Zhou, H., Zhao, J.P., Loo, C.E., Ellis, B.G. and Cen, K.F., 2012. Model predictions of important bed and gas properties during iron ore sintering. *ISIJ international*, *52*(12), pp.2168-2176.